Spiral Defect Chaos in Rayleigh-Bénard Convection

W. Decker, W. Pesch, and A. Weber
Physikalisches Institut der Universität Bayreuth, 95440 Bayreuth, Germany
(Received 15 February 1994)

Motivated by recent experiments on Rayleigh-Bénard convection, where spiral defect chaos was discovered, we have simulated the Boussinesq equations for the appropriate Rayleigh numbers not far from threshold for large aspect ratio systems using a Galerkin method. A detailed analysis of the results reproduces the experimental findings almost quantitatively. A critical comparison with recent model calculations is also presented. Our investigations show that the new spatiotemporal pattern must be considered generic for Rayleigh-Bénard convection.

PACS numbers: 47.10.+g, 47.20.Bp

Rayleigh-Bénard convection (RBC) in a fluid layer heated from below provides a canonical example for pattern-forming transitions in nonequilibrium fluid systems [1,2]. The convection sets in if the temperature difference ΔT across the fluid layer, characterized by the nondimensional Rayleigh number R, exceeds a certain threshold ΔT_c ($R = R_c$). Above onset the Prandtl number Pr= ν/κ, where ν is the kinematic viscosity and κ the thermal diffusivity becomes important. The stability regimes (the "Busse balloon") of periodic parallel-roll patterns with wave vectors $\mathbf{q}$ in the R-Pr space have been classified by Busse and co-workers [3]. However, the natural textures are often found to be more complicated [4,5] and very recently a new fascinating spatiotemporal pattern was described consisting of many right and left handed rotating spirals besides other defects ("spiral defect chaos") [6,7]. The fully developed state appeared in a circular cell with large aspect ratio (Γ = radius/height $\approx$ 80) filled with gaseous CO_2 (Pr$\approx$ 1) fairly near to onset of convection [$\epsilon = (R - R_c)/R_c \gtrsim 0.5$]. The corresponding average wave number $q_{\rm av}$ lies near the center of the stable wave number band of parallel rolls.

In order to provide for a well-founded theoretical description of the new scenario, we present in this Letter simulations based on the standard theoretical description of RBC, namely, the well-known Boussinesq equations (see, e.g., [1–3,8]). One has a nonlinear coupling between the velocity field $\mathbf{u}$ (Navier-Stokes equations) and the deviation θ of the temperature from the linear static profile (heat diffusion equation). For a reduction to nondimensional form (containing only the Rayleigh number R and the Prandtl number Pr) lengths are measured in units of the cell thickness d and time in units of the vertical diffusion time $t_v \equiv d^2/\kappa$. We consider realistic rigid boundary conditions ($\theta = \mathbf{u} = 0$ at the horizontal boundaries $z = \pm\frac{1}{2}$). The onset of convection is then at $R_c = 1707.37$. Because of isotropy only the modulus of the critical wave vector $\mathbf{q}_c$ ($q_c = 3.12$) is fixed.

According to [3] a poloidal-toroidal decomposition of the solenoidal vector field $\mathbf{u}$ has been used,

$$\mathbf{u} = (\partial_{xz}, \partial_{yz}, -\partial_{xx} - \partial_{yy})\, f + (\partial_y, -\partial_x, 0)\, g. \qquad (1)$$

Because of its nonzero spatial average across the cell, the toroidal part g is often interpreted in terms of "mean flow" or "mean drift" effects. Using the standard Galerkin technique to satisfy the horizontal boundary conditions, f is expanded in terms of Chandrasekhar functions $C_n(z)$ and θ, g in terms of trigonometric functions (or polynomials) with respect to z [3]. In a minimal description the expansion has been truncated as follows:

$$\theta(\vec{r}, z) = \theta_1(\vec{r}) \sin\left(\pi(z + \tfrac{1}{2})\right) + \theta_2(\vec{r}) \sin\left(2\pi(z + \tfrac{1}{2})\right),$$
$$f(\vec{r}, z) = f_1(\vec{r}) C_1(z) + f_2(\vec{r}) C_2(z),$$
$$g(\vec{r}, z) = g(\vec{r})(z^2 - \tfrac{1}{4}).$$

By subsequent projection onto the vertical modes one arrives at a coupled system for the five coefficient functions of the horizontal coordinate $\vec{r}$.

The truncation of the z modes should be of minor importance for the spiral chaos. In fact, in Fig. 1 it is demonstrated that in this approximation the Busse balloon is reproduced quite accurately, a prerequisite for any trustworthy treatment of the problem. A further decisive simplification is possible. The experimental results [6] show that spiral chaos is described in Fourier space by modes with wave vectors $\mathbf{q}$ lying in an annulus, where $|\mathbf{q}|$ stays virtually within the stability boundaries in Fig. 1. Nonlinear interactions lead to the excitation of modes

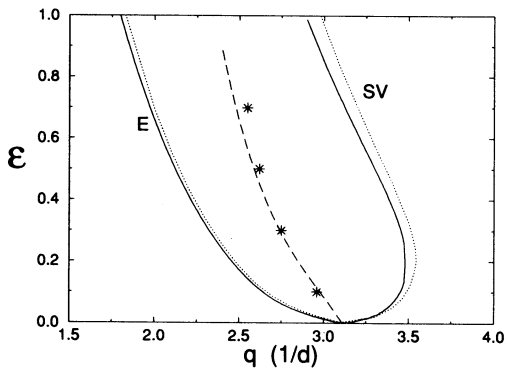

FIG. 1. The Busse balloon for Pr= 1 (dotted line: rigorous computations; solid line: 5 mode approximation). Included is the average wave number $q_{\rm av}(\epsilon)$ of the patterns from experiments (dashed line) [6] and from simulations (stars).

0031-9007/94/73(5)/648(4)$06.00

with much smaller weight at $q \approx 0$ and $q \approx 2q_c$. A cutoff in wave number space at $q_m \approx 2.5q_c$ turns out to be sufficient.

Since we were interested in generic features, the resulting equations have been simulated mainly in a square with linear dimension L and periodic boundary conditions in the horizontal ($\vec{r}$) directions. All derivatives are performed in Fourier space and the nonlinearities are evaluated by pseudospectral methods and fast Fourier transformation (FFT). To solve for the time dependence we have chosen a fully implicit scheme for the linear terms, whereas the nonlinear parts have been treated explicitly (second order Adam-Bashforth method). The typical time step was $\lesssim 0.04t_v$ (t_v ca. 1.3 sec in the experiments [6]). The results presented below are mostly based on $N = 256$ Fourier modes in each horizontal direction for the five coefficient functions. The FFT was typically truncated at $q_m = 2.5q_c$ corresponding to an aspect ratio $\Gamma = \frac{L}{2d} = \frac{N\pi}{2q_m}$ (i.e., $\Gamma \approx 50$ for $N = 256$). Even runs on a 128×128 mesh ($\Gamma \approx 25$) already reveal a chaotic spiral state, with less than three spirals on the average in the cell. We have checked our results by changing the time steps, the cutoff q_m (up to $5q_c$), and N (also time consuming runs with $N = 512$ were performed).

In Fig. 2(a) a typical snapshot at $500t_v$ ($\Gamma = 50$) is shown, generated by small random initial conditions for $\epsilon = 0.7$, which apparently reproduces all experimental features [see Fig. 2(b)]. The initial buildup of a spiral pattern ("temporal change of the amplitude") was surprisingly fast ($< 30t_v$). The typical time scale of the subsequent persistent dynamics, judged from visible changes of the patterns ("temporal change of the phase"), was estimated to be $20t_v$, in agreement with the experiments [9].

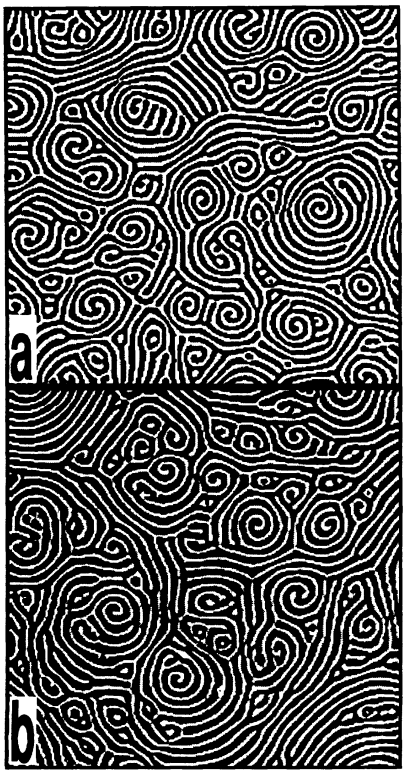

FIG. 2. Snapshots of the temperature field θ_1 from simulations (a) at ϵ=0.7, Pr= 1 compared with experimental results (b) (ϵ=0.72, Pr=0.96) (with courtesy from [6]).

The patterns (for smaller ϵ see below) have been analyzed quantitatively in close analogy to the experimental work [6]. At first the mean wave vector $q_{\rm av}(\epsilon)$ was extracted from $\overline{S}(q)$, defined as the azimuthal and time average of the structure function $S(\mathbf{q}) = |\theta_1(\mathbf{q})^2|$. Our values of $q_{\rm av}$ coincide well with the experimental results (see Fig. 1). The Lorentz-type wave vector distribution $\overline{S}(q)$ shown in Fig. 3 for $\epsilon = 0.7$ seems to respect the two border lines of the Busse balloon. The inverse width ξ of $\overline{S}(q)$ as a function of ϵ is in excellent agreement with the experimental result $\xi = 2.4\epsilon^{-0.43}d$ [6]. The time consuming analysis of the dynamical structure function has been performed only for $\epsilon = 0.7$ and revealed rather an exponential decay with a correlation time $\tau_{\rm cor} \approx 18t_v$ at the maximum of $\overline{S}(q)$ [the experiments yield $(13 \pm 3)t_v$ [9]].

We have tried to get an impression of the spiral-defect-chaos attractor by changing ϵ and the initial conditions. Above $\epsilon \gtrsim 0.5$, for $N = 256$, one always gets to spiral chaos as long as no preferred direction is singled out (e.g., starting from random initial conditions or from a collection of roll patches with different orientations in space). Below $\epsilon \lesssim 0.5$ the system develops into clearly different plan forms with very few defects (dislocations, grain boundaries) with $q_{\rm av}(\epsilon) < q_c$. The appearance of spiral chaos is also correlated with the aspect ratio Γ; it is found for $\epsilon \gtrsim 0.45$ if $\Gamma = 100$ and for $\epsilon \gtrsim 0.65$ if $\Gamma = 25$, a tendency in agreement with experiments [7]. There is no difference when the simulations are confined to a large circular domain [10] and the characteristic snapshots for different ϵ shown in Fig. 4 are very similar to the corre-

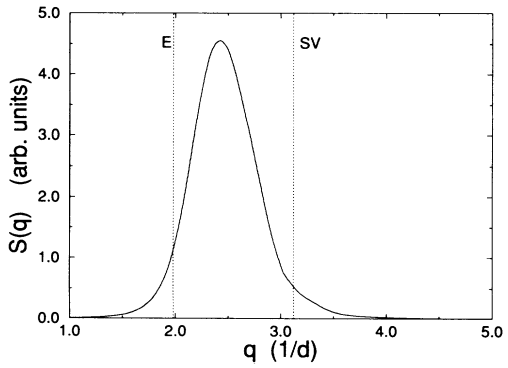

FIG. 3. Wave vector distribution $\overline{S}(q)$ for $\epsilon = 0.7$. Included are the corresponding Eckhaus (E) and the skewed-varicose (SV) limits.

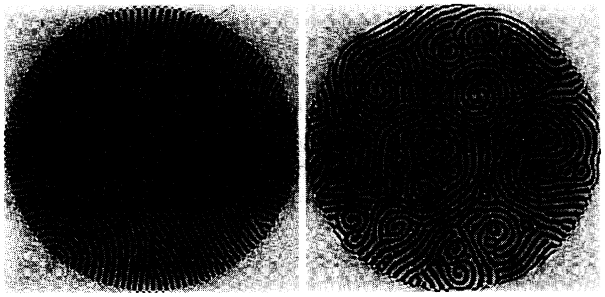

FIG. 4. Snapshots of the temperature field θ_1 from simulations for $\epsilon = 0.3$ (left) and $\epsilon = 0.7$ (right) (Pr= 1.0).

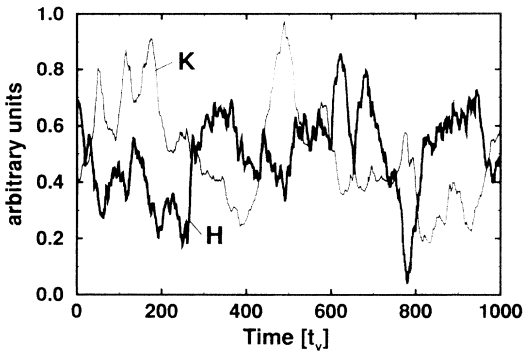

FIG. 5. Kinetic energy K of the mean flow and the convective heat current H for $\epsilon = 0.7$ and $N = 128$. The mean value of both quantities is shifted to 0.5, with otherwise arbitrary units.

sponding experimental ones [6]. But the scenario changes drastically, if one initially imposes a preferred direction, e.g., a periodic roll pattern. Even an initial superposition of noise with a strength of 80% of the roll amplitude is not sufficient to prevent the eventual recovery of the stable roll-pattern attractor at $\epsilon = 0.7$.

The typical persistent dynamical behavior of the convective heat flux H [proportional to $\theta_2(q = 0)$] and the "kinetic energy" K of the mean flow [spatial average of $|\nabla g(\vec{r})|^2$] (see [11,12]) for a small circular cell ($\Gamma = 25$) with spiral chaos is shown in Fig. 5. The heat flux is reduced on the average by 25% in comparison to the ideal roll-pattern case with maximal fluctuations of the order of 3% on a time scale of the order of the horizontal diffusion time $t_h = \Gamma^2 t_v$. In analogy to Refs. [11,12] H and K are often anticorrelated, where an increase of K is related to fairly free moving spirals, which then get captured and destroyed at the boundaries, a process also found for other defects in experiments [4,13,14].

There is no doubt that the coupling to the mean flow (g), which is proportional to Pr^{-1} and increases roughly proportional to ϵ, is crucial for spiral chaos at medium Pr [and also for the correct shape of the Busse balloon with respect to the skewed-varicose (SV) instability line [3,15]]. Merely frozen-in labyrinthic patterns were observed at large Pr (= 6) or when g was disregarded. The field g, which has extrema at the positions of the spirals and also becomes large where rolls bend strongly [11], has not been plotted, because it gave no further insight at the moment.

Our approach also allowed us to deduce a kind of minimal description, which reproduces essentially the above results. Focusing on the amplitudes $A(\mathbf{q}, t)$ of the fastest growing modes above threshold turned out to be satisfactory, whereas all other modes are slaved adiabatically. $A(\mathbf{q}, t)$ is then determined by an order parameter equation in Fourier space [16]. A transformation to real space becomes possible, if singular terms in the ensuing gradient expansion are absorbed systematically in a separate equation for g [17,18]. Unfortunately one needs in addition a large number of gradient terms in the cubic nonlinearities of the resulting generalized Newell-Whitehead equations [19] to map the Busse balloon accurately up to $\epsilon \approx 1$ [18].

The first to point out the importance of mean-flow effects and isolate them explicitly in the amplitude-equation formalism were Siggia and Zippelius [20] in the case of stress free boundary conditions (see also [21]). Later on isotropic generalizations of the amplitude equations [of the Swift-Hohenberg (SH) type [22], but including mean-flow effects] were introduced [23,24] which exhibit complex spatiotemporal behavior [11,25]. In recent remarkable papers [26,27] it was shown that also the scenario of spiral chaos is contained in model equations of the SH type. A quantitative comparison with the experiments by adjusting the model parameters [27] is not quite conclusive in our opinion [28]. First, the strength of the coupling to g is overestimated by a factor of about 4 [29], which might explain the appearance of the spiral chaos already at $\epsilon \approx 0.25$ in contrast to the experiments. Moreover, the stability balloon is dissimilar to the correct one [30]. In particular the SV line does not bend back with increasing ϵ (see Fig. 1). More serious is the occurrence of an unphysical short-wavelength cross roll instability in the model, which renders almost the whole regime $q > q_c$ unstable. This also pushes q_{av} to the left, but too strongly ($q_{\mathrm{av}} \approx 0.8 q_c$ instead of $0.92 q_c$ at $\epsilon = 0.25$ in the experiments). Nevertheless, these model calculations are of considerable importance, since they show that the scenario of spiral chaos is of surprising robustness.

In conclusion, we have shown by detailed evaluation of our simulations (in comparison with the experiments) that the spiral chaos is an intrinsic attractor of the Boussinesq equations. This state is attained most easily starting from random initial conditions, if the aspect ratio is not too small. At least for Pr$\approx$ 1 we strongly believe that a cooperative interaction between roll curvature and mean flow (some ingredients of which are described lucidly in [11]) is responsible for the persistent defect dynamics. It is important that in view of our calculational method further theoretical analysis will be

simplified considerably. Our results show that the vertical structure of the fields is not crucial and that periodic boundary conditions can be used. It is also important that the so called non-Boussinesq (NB) effects (temperature dependence of material parameters, which destroy the up-down symmetry [31]) need not be taken into account, at least for Pr$\sim$ 1.

To characterize a more specific mechanism for the occurrence of the spiral-defect-chaos attractor and in particular under which conditions it is likely to show up in the experiments at the expense of the periodic roll patterns, further time-consuming simulations are necessary. In addition, we plan to implement NB effects into our treatment, which would also allow us to assess the competition between spirals and hexagons [26,32,33]. Then also the "many target" and spiral patterns, observed at larger ϵ and Pr, whose existence is tentatively attributed to NB effects [34], should be found.

We would like to thank F. Busse, H. Brand, L. Kramer, and I. Rehberg for illuminating discussions. We are in addition very grateful to L. Kramer for carefully reading the manuscript. We are further indebted to G. Ahlers, E. Bodenschatz, and S. Morris for numerous suggestions, detailed information about the experiments, and for providing their data. Our investigations were encouraged by a very fruitful discussion with E. Siggia who suggested solving the Boussinesq equations directly instead of model equations.

[1] P. Manneville, *Dissipative Structures and Weak Turbulence* (Academic, New York, 1990).
[2] M. C. Cross and P. C. Hohenberg, Rev. Mod. Phys. **65**, 851–1112 (1993).
[3] F. H. Busse, in *Hydrodynamic Instabilities and the Transition to Turbulence*, edited by H. L. Swinney and J. P. Gollub (Springer, Berlin, 1986).
[4] V. Croquette, Contemp. Phys. **30**, 113 (1989); **30**, 153 (1989).
[5] A. C. Newell, T. Passot, and J. Lega, Annu. Rev. Fluid Mech. **25**, 399 (1993).
[6] S. W. Morris, E. Bodenschatz, D. S. Cannell, and G. Ahlers, Phys. Rev. Lett. **71**, 2026 (1993).
[7] Y. Hu, R. Ecke, and G. Ahlers, Phys. Rev. E **48**, 4399 (1993).
[8] A. V. Getling, Usp. Fiz. Nauk. **161**, 1 (1991) [Sov. Phys. Usp. **34**, 101 (1991)].
[9] S.W. Morris, E. Bodenschatz, G. Ahlers, and D.S. Cannell (to be published).
[10] In a fairly crude manner we have simulated a circular container of radius r by putting all fields to zero in position space outside r at each time step.
[11] P. Manneville, J. Phys. (Paris), Lett. **44**, L903 (1983).
[12] F. H. Busse, Contemp. Math. **56**, 1 (1986).
[13] A. Pocheau, V. Croquette, and P. Le Gal, Phys. Rev. Lett. **55**, 1094 (1985).
[14] V. Steinberg, G. Ahlers, and D. Cannell, Phys. Scr. **32**, 534 (1985).
[15] M. C. Cross and A. C. Newell, Physica (Amsterdam) **10D**, 299 (1984).
[16] H. Haken, *Synergetics* (Springer-Verlag, Berlin, 1978).
[17] M. Kaiser and W. Pesch, Phys. Rev. E **48**, 4510 (1993).
[18] W. Decker and W. Pesch, J. Phys. (France) (to be published).
[19] A. C. Newell and J. A. Whitehead, J. Fluid Mech. **28**, 279 (1969).
[20] E. D. Siggia and A. Zippelius, Phys. Rev. Lett. **47**, 835 (1981).
[21] M. C. Cross, Phys. Rev. A **27**, 490 (1983).
[22] J. B. Swift and P. C. Hohenberg, Phys. Rev. A **15**, 319 (1977).
[23] P. Manneville, J. Phys. (Paris) **44**, 759 (1983).
[24] H. S. Greenside and M. C. Cross, Phys. Rev. A **31**, 2492 (1985).
[25] H. S. Greenside, M. Cross, and W. M. Coughran, Phys. Rev. Lett. **60**, 2269 (1988).
[26] M. Bestehorn, M. Fantz, R. Friedrich, and H. Haken, Phys. Lett. A **174**, 48 (1993).
[27] H. W. Xi, J. D. Gunton, and J. Viñals, Phys. Rev. Lett. **71**, 2030 (1993).
[28] In agreement with experiments the dynamics is much faster than assumed in [27], because time is measured there in units of $[4\tau_0/(q_c\xi_0)^2]\,t_v = 0.2t_v$ (at Pr=1) instead of t_v.
[29] That number can be deduced without difficulty from P. Manneville and J. M. Piquemal, Phys. Rev. A **28**, 1714 (1983) (see also [18]).
[30] The stability diagram looks similar to Figs. 8 and 9 of [24].
[31] F. H. Busse, J. Fluid Mech. **30**, 625 (1967).
[32] E. Bodenschatz, J. R. de Bruyn, G. Ahlers, and D. S. Cannell, Phys. Rev. Lett. **67**, 3078 (1991).
[33] H. W. Xi, J. D. Gunton, and J. Viñals, Phys. Rev. E **47**, R2987 (1993).
[34] M. Assenheimer and V. Steinberg, Phys. Rev. Lett. **70**, 3888 (1993); Nature (London) **367**, 345 (1994).

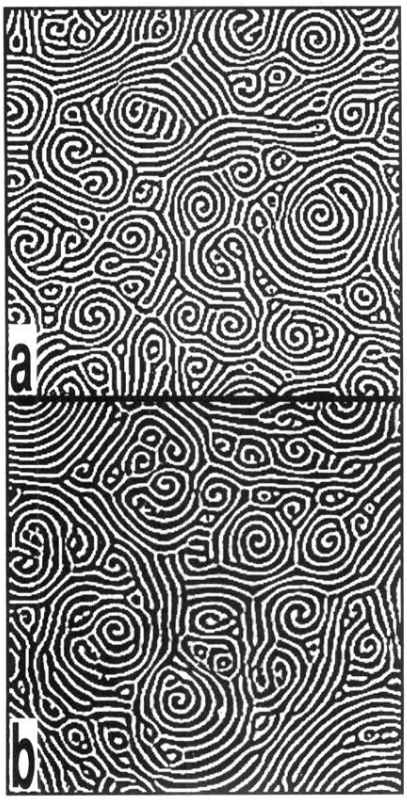

FIG. 2. Snapshots of the temperature field θ_1 from simulations (a) at ϵ=0.7, Pr= 1 compared with experimental results (b) (ϵ=0.72, Pr=0.96) (with courtesy from [6]).

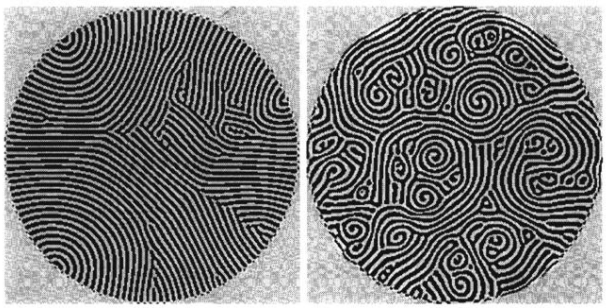

FIG. 4. Snapshots of the temperature field θ_1 from simulations for $\epsilon = 0.3$ (left) and $\epsilon = 0.7$ (right) (Pr= 1.0).